

Statistical γ decay of the giant dipole resonance in highly excited ^{46}Ti and ^{52}Cr

G. Feldman,* K. A. Snover, J. A. Behr,[†] C. A. Gossett, J. H. Gundlach, and M. Kicińska-Habior[‡]
Nuclear Physics Laboratory, University of Washington, Seattle, Washington, 98195

(Received 28 April 1992)

We have measured inclusive γ -ray spectra from the reactions $\alpha + ^{48}\text{Ti} \rightarrow ^{52}\text{Cr}$ and $^{19}\text{F} + ^{27}\text{Al} \rightarrow ^{46}\text{Ti}$, populating final states at moderate temperature and spin. These spectra were analyzed using a statistical model including giant resonance strength functions in the γ -decay width. The parameters of the giant dipole resonance (GDR) strength function were varied to fit the data. Two different level-density formulations were utilized—one (Pühlhofer) in which the level-density parameters were adjusted to obtain the best overall fit to the data, and the other (Reisdorf) which contained no free parameters. While the magnitudes of the extracted GDR parameters differed in the two cases, their dependence on final-state energy was similar. The GDR energy was observed to be nearly constant with the final-state energy, and the GDR strength exhausted nearly a full $E1$ sum rule. In the $\alpha + ^{48}\text{Ti}$ reaction, the GDR width was observed to increase slightly with increasing bombarding energy. In the $^{19}\text{F} + ^{27}\text{Al}$ reaction, a pronounced GDR width increase was observed with increasing bombarding energy and was attributed to an increase in compound nucleus spin. These results are consistent with current calculations based on the rotating liquid-drop model and with recent experimental reports.

PACS number(s): 21.10.Ma, 24.30.Cz, 27.40.+z, 25.55.-e

I. INTRODUCTION

Statistical γ decay of the giant dipole resonance (GDR) in highly excited compound nuclear systems has recently been of interest in medium and heavy nuclei. These studies have provided valuable information on dynamic properties, especially the deformation of compound nuclei at moderate temperature and spin [1–9]. However, very little work has been performed on relatively light ($A < 70$) systems (exceptions are Refs. [10–12]).

In the current paper, we have studied the high-energy γ decay of the compound nuclei ^{46}Ti and ^{52}Cr formed in fusion reactions. We have measured inclusive γ -ray spectra from the fusion reactions $^{19}\text{F} + ^{27}\text{Al}$ and $\alpha + ^{48}\text{Ti}$ in order to investigate the statistical decay of the GDR in these highly excited compound nuclei. Our motivation was to observe the effects of excitation energy, spin, and isospin on the statistical decay of these relatively light compound systems. These nuclei were also studied in (p, γ) reactions [13], hence the present measurements also serve to achieve a quantitative understanding of statistical γ -ray emission relevant to the interpretation of the (p, γ) data populating the same nuclei.

These fusion reactions were measured at four bombarding energies. The $\alpha + ^{48}\text{Ti}$ system was studied at $E_\alpha = 12, 17.2, 24,$ and 28 MeV, corresponding to initial

compound nucleus excitation energies $E_{xi} = 20.4, 25.2, 31.5,$ and 35.2 MeV. The $^{19}\text{F} + ^{27}\text{Al}$ reaction was measured at $E(^{19}\text{F}) = 30, 40, 50,$ and 60 MeV, corresponding to $E_{xi} = 42.5, 46.8, 52.0,$ and 58.1 MeV. In addition, five-point angular distributions were obtained at $E_\alpha = 17.2$ and 24 MeV and $E(^{19}\text{F}) = 60$ MeV to serve as a model-independent test of the assumption of statistical GDR decay.

The results of this work indicate that the GDR energy is roughly constant over the range of excitation energies studied, and the resonance strength is generally within 20% of a full $E1$ sum rule. The GDR width tends to increase with higher bombarding energy, and in the case of the $^{19}\text{F} + ^{27}\text{Al}$ reaction, this width increase was identified as most likely due to a spin-induced increase in the nuclear deformation which is unresolved in the spectrum shape.

II. EXPERIMENTAL DETAILS

The experiments were conducted at the University of Washington, using alpha and ^{19}F beams from the FN tandem Van de Graaff accelerator. Targets were self-supporting rolled foils of ^{27}Al metal and ^{48}Ti metal (isotopically enriched to 99%). The target thicknesses, as measured by energy loss of 5.486 MeV α particles from an ^{241}Am source, were determined within $\pm 5\%$ to be 1.39 and 0.98 mg/cm², respectively.

Capture γ rays were detected in a 25.4 cm \times 25.4 cm NaI(Tl) detector with an active anticoincidence shield [14]. The central NaI crystal was surrounded by ~ 2 cm of ^6LiH to absorb thermal neutrons. The entire spectrometer assembly was surrounded by 10 cm of Pb shielding on the front and sides, as well as 36.4 cm of wax in front to moderate fast neutrons coming from the target. The front face of the NaI detector was located 73.7 cm

*Present address: Saskatchewan Accelerator Laboratory, University of Saskatchewan, Saskatoon, Saskatchewan, Canada S7N 0W0.

[†]Present address: Department of Physics, SUNY at Stony Brook, Stony Brook, NY 11794.

[‡]Permanent address: Institute of Experimental Physics, University of Warsaw, 00-681 Warsaw, Poland.

from the target. The spectral shape measurements were performed at $\theta_\gamma=90^\circ$, and the angular distributions were measured at $\theta_\gamma=40^\circ, 55^\circ, 90^\circ, 125^\circ$, and 140° .

To ensure stable gain over the course of the data collection, the NaI detector was equipped with transistorized phototube bases, and a light pulser feedback system was used to monitor the reference position of an LED signal and correct the NaI high-voltage power supply. This method of gain stabilization has been shown to be reliable to better than 0.5% over periods of several days [15]. The absolute energy calibration was deduced from the following set of γ -ray lines: 22.61 and 18.17 MeV from states in ^{12}C via the $^{11}\text{B}(p,\gamma)^{12}\text{C}$ reaction at $E_p=7.25$ MeV; 5.02, 4.45, and 2.90 MeV from ^{11}B inelastic proton scattering; and 6.13 and 2.23 MeV from a ^{13}C -Pu source. After fixing the detector gain calibration at the beginning of each running period, the gain was checked periodically to verify that no gain drift had occurred.

To discriminate neutron events from γ -ray events in the NaI detector, it was necessary to perform time-of-flight measurements with pulsed beam. A time resolution of 3–5 ns was obtained for a wide range of γ -ray energies in the NaI and was sufficient to achieve a clear time separation of neutron and γ -ray events. Pileup rejection was particularly important in these measurements, since the essentially structureless character of the spectra makes it difficult to discern pileup effects. Pileup was suppressed by fast pileup-rejection electronics ($\sim 50\%$ efficiency), and a separate off-line subtraction was performed to eliminate any residual pileup events from the spectrum. All runs required measuring spectra down to $E_\gamma \sim 3$ MeV and were performed in pulsed-beam mode at low counting rates (~ 15 – 25 kHz above 0.25 MeV). This technique leads to a further suppression of cosmic-ray background by about a factor of 40, due to the pulsed-beam duty factor of $1/(240\text{ ns})$.

III. DATA ANALYSIS AND RESULTS

Absolute cross sections for the γ -ray spectra were deduced based on knowledge of the target thickness, total accumulated charge, dead time, solid angle, and efficiency of the NaI detector. Angle-integrated cross sections were obtained by assuming an isotropic angular distribution (see Sec. III D below). The energy dependence of the NaI efficiency was determined by direct measurement [16] for $E_\gamma \leq 15.1$ MeV and by calculations using the EGS4 electron-gamma shower code [17] for higher energies. Over the energy range of the current work, the efficiency is known to $\pm 5\%$. Because the detector response to monoenergetic photons involves a photopeak plus a low-energy tail, the spectra cannot be converted to cross section without deconvoluting the detector response function. Instead, we analyze the statistical decay spectra by folding the NaI line shape into the statistical-model calculation and comparing directly with the measured yield. In this manner, the energy-dependent detector response is properly taken into account. The results are shown in Figs. 1 and 4. The vertical scale is determined by the value of the detector efficiency at $E_\gamma=15.1$ MeV and hence is (exactly) correct at this energy. Since the efficiency varies slowly with energy, the cross section scale determined in this manner is accurate to $\sim 10\%$ for γ -ray energies between 7 and 25 MeV.

The γ -ray spectra were analyzed using the statistical-model code CASCADE [18]. With the premise that the fusion reaction forms a highly excited compound nucleus in thermal equilibrium, CASCADE calculates relative decay widths for light particle (n, p, α) and γ -ray emission, generating population matrices for the parent and daughter nuclei as a function of excitation energy and spin. This procedure continues through all possible sequences in the decay cascade. The initial spin distribution of the compound nucleus is determined from the

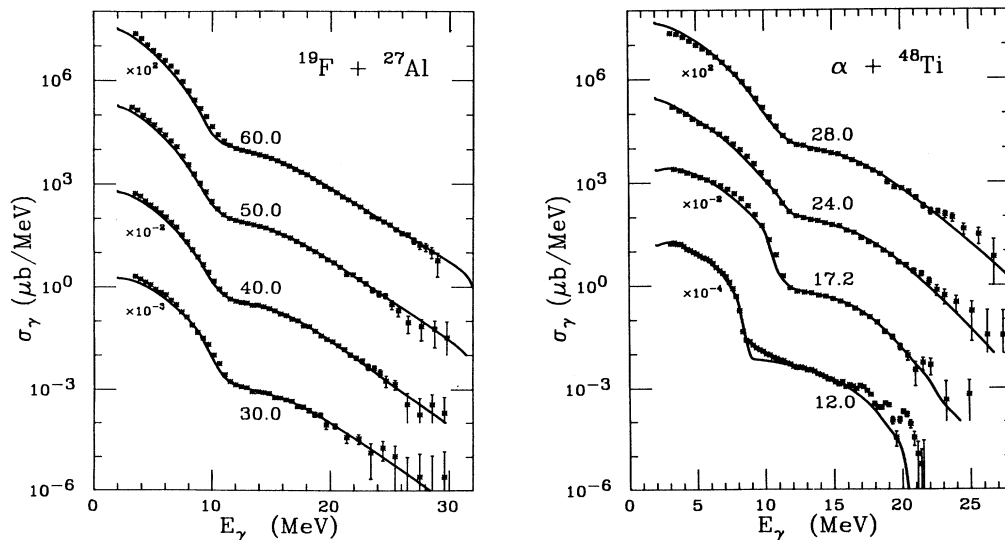


FIG. 1. Measured inclusive γ -ray spectra at $\theta_\gamma=90^\circ$ for the $^{19}\text{F}+^{27}\text{Al}$ reaction at $E(^{19}\text{F})=60, 50, 40$, and 30 MeV (left panel) and for the $\alpha+^{48}\text{Ti}$ reaction at $E_\alpha=28, 24, 17.2$, and 12 MeV (right panel). The solid curves are CASCADE statistical-model fits using the Pühlhofer level-density formulation with parameters $a=A/8.5$ and Δ including the Wigner term.

strong-absorption model. The decay probabilities are computed from the Hauser-Feshbach formulas [19] which include level densities of final states and transmission coefficients for particle decay channels. Details of the statistical theory of nuclear reactions have been given elsewhere (e.g., Refs. [20–22]).

In general, the decay width for emitting a γ ray of energy E_γ and multipolarity L is:

$$\frac{d\Gamma_\gamma(E_\gamma)}{dE_\gamma} = \frac{\rho(E_{xf}, J_f, \pi_f)}{\rho(E_{xi}, J_i, \pi_i)} \sum_L f_{EL}(E_\gamma) E_\gamma^{2L+1}, \quad (1)$$

where $E_\gamma = E_{xi} - E_{xf}$ and $\rho(E, J, \pi)$ is the level density, which depends on excitation energy, spin, and parity. The γ -decay width includes a GDR strength function for $E1$ transitions, and both isovector and isoscalar giant quadrupole resonance components for $E2$ transitions [23]. Following the Brink hypothesis [24] which states that the form of the GDR built on excited states is the same as the ground-state case, the GDR was represented by a Lorentzian shape:

$$f_{E1}(E_\gamma) = \frac{2}{3\pi} \frac{1}{(\pi\hbar c)^2} S \left[60 \frac{NZ}{A} \text{ MeV mb} \right] \times \frac{E_\gamma \Gamma}{(E_0^2 - E_\gamma^2)^2 + E_\gamma^2 \Gamma^2}, \quad (2)$$

with peak energy E_0 , width Γ , and strength S (in units of the classical dipole sum rule). A least-squares fitting version of CASCADE was employed to vary the GDR parameters (E_0 , Γ , and S) in order to minimize χ^2 over a specified region of the γ -ray spectrum. The fitting interval extended from $E_\gamma \sim 10$ –12 MeV up to the highest E_γ values—this is the region most sensitive to the GDR parameters.

The inclusive γ -ray spectra for the $^{19}\text{F}+^{27}\text{Al}$ and $\alpha+^{48}\text{Ti}$ reactions are plotted in Fig. 1. The smooth monotonic shapes are characteristic of statistical GDR decays from highly excited compound nuclei. The GDR “bump” is evident above $E_\gamma \sim 11$ MeV and extends up to 30 MeV—it is in this region of the spectrum where high-energy γ emission competes directly with low-energy particle evaporation. The intense low-energy γ yield arises from deexcitation of daughter nuclei populated at an energy which is below the particle binding energy plus the yrast energy. The solid curves are the results of the statistical-model calculations described in more detail below.

A. Fusion cross sections

Under the assumption of a completely equilibrated compound system, the entrance channel matters only insofar as it determines the initial excitation energy and spin distribution of the compound nucleus. The partial cross section $\sigma(J)$ is given by:

$$\sigma(J) = \pi\lambda^2 \frac{2J+1}{(2J_p+1)(2J_t+1)} \sum_{s=|J_t-J_p|}^{|J_t+J_p|} \sum_{l=|J-s|}^{|J+s|} T_l(E), \quad (3)$$

where J_p and J_t are the projectile and target spins, s is the channel spin, and l is the orbital angular momentum. The total fusion cross section is given by the sum over J of all the partial cross sections. In the normal CASCADE code, transmission coefficients $T_l(E)$ are approximated in the strong-absorption limit by a Fermi function. Since the overall magnitude of the calculated γ -ray cross section is determined by the fusion cross section, this was adjusted in the present work to give the proper yield of low-energy γ rays. For the α -induced reactions, the fusion cross sections were computed using transmission coefficients $T_l(E)$ taken from optical-model results [25], rather than using the strong-absorption approximation typically employed in heavy-ion reactions. The resulting fusion cross sections agreed well with the data with no need for adjustment, except for the case of $E_\alpha = 12$ MeV, which needed to be reduced by a factor of 0.7. For the other α energies, comparisons with α -induced reactions on neighboring nuclei [26,27] confirmed that the above values were within 20% of published results.

A special concern for the ^{19}F reactions was the large energy loss (~ 10 MeV) in the ^{27}Al target. For $E(^{19}\text{F}) = 50$ and 60 MeV, CASCADE calculations revealed that the spectrum shape and magnitude changed only slightly over the range of beam energy loss; therefore, the average beam energy in the target was used as the effective bombarding energy in the CASCADE fits. For $E(^{19}\text{F}) = 40$ MeV, the calculated shape was still insensitive to the energy loss, but the magnitude varied by more than a factor of three; in this case, the effective bombarding energy was deduced by averaging over the target thickness weighted by the fusion cross section. Comparison of the calculated spectrum shape for this effective bombarding energy with the calculated shape averaged over the beam energy loss verified the validity of this procedure. In all of the above reactions, however, to reproduce the low-energy part of the spectrum required σ_{fus} values that were ~ 20 –40% higher than the published measurements [18,28].

Such a change in the fusion cross section affected only the GDR strength in a non-negligible way. The energy and width obtained from fits using the published σ_{fus} values differed by less than 2% and the strengths differed by $\sim 12\%$ from the results obtained by the above procedure. The strength does not scale exactly with σ_{fus} because larger values of σ_{fus} correspond to larger initial spins, for which the probability of high-energy γ decay is less than for low spins.

While discrepancies in the fusion cross section have been shown to have a small effect on the GDR parameters, there may be some concern that other mechanisms (besides fusion evaporation) could contribute to the γ -ray spectra. This question has been addressed for very similar entrance channels in Ref. [10], where possible distortions due to deep-inelastic scattering and heavy-ion bremsstrahlung were argued to be negligible.

The case of $E(^{19}\text{F}) = 30$ MeV is very close to the Coulomb barrier and was beyond the capability of CASCADE to compute an initial spin distribution. This problem was resolved by appealing to the barrier penetration model developed by Wong [29]. Here the transmission

TABLE I. Entrance channel information for the reactions studied in the present work. V_b is the Coulomb barrier in the c.m. system, and E_{xi} is the initial compound nucleus excitation energy. The mean initial spin $\langle J_i \rangle$ was computed by averaging over the assumed compound nucleus spin distribution. The fusion cross sections σ_{fus} are the values used in the current analysis.

Reaction	Q value (MeV)	V_b (MeV)	E_{lab} (MeV)	$E_{\text{c.m.}}$ (MeV)	E_{xi} (MeV)	$\langle J_i \rangle$ (\hbar)	σ_{fus} (mb)
$\alpha + {}^{48}\text{Ti}$	9.35	7.2	28.0	25.8	35.2	9.3	1440
			24.0	22.2	31.5	8.4	1380
			17.2	15.9	25.2	6.5	1190
			12.0	11.1	20.4	4.5	570
${}^{19}\text{F} + {}^{27}\text{Al}$	25.44	17.2	55.7	32.7	58.1	19.1	1460
			45.3	26.6	52.0	14.3	960
			36.4	21.4	46.8	8.6	360
			29.0	17.0	42.5	3.5	13

coefficients $T_l(E)$ are computed according to the Hill-Wheeler formula [30] assuming a parabolic shape for the peak of the interaction (nuclear plus Coulomb) potential. The relevant parameters are the barrier height $V_b = 17.2$ MeV and interaction radius $R_b = 8.1$ fm given by fusion data [28] and the curvature $\hbar\omega = 3.5$ MeV calculated from the second derivative of the potential (Eq. (6) in Ref [29]) with appropriate optical-model parameters. We obtained $\hbar\omega$ from optical potentials fitted to elastic scattering of ${}^{18}\text{O}$ [31] and ${}^{20}\text{Ne}$ [32] on ${}^{27}\text{Al}$. The effective bombarding energy (and hence the initial spin distribution) was determined by a weighted average of projectile energies through the target.

Table I lists the reactions and bombarding energies covered in the present work, along with the initial excitation energy E_{xi} and the fusion cross section σ_{fus} used in the CASCADE calculations. The mean initial spin $\langle J_i \rangle$ was computed by averaging over the assumed compound nucleus spin distribution consistent with σ_{fus} .

B. Isospin and parity

The normal version of CASCADE ignores isospin and treats parity in an approximate way. In a more recent version of the CASCADE code, Harakeh *et al.* [12] have included the proper formalism to perform statistical-model calculations in good isospin and parity. The impact of these considerations was investigated by comparing results obtained from fits with both versions of the statistical-model code. For the ${}^{19}\text{F} + {}^{27}\text{Al}$ reaction, both versions gave similar GDR energies, and the widths differed only slightly ($\sim 6\%$). The dominant effect, however, was a strength increase, by factors of ~ 1.7 for $E({}^{19}\text{F}) \geq 40$ MeV and ~ 2.0 for $E({}^{19}\text{F}) = 30$ MeV. This significant increase is largely due to the isospin-dependent γ -ray transmission coefficients used in the code. For the α -induced reactions, the extracted energies and widths were unchanged within errors, and the strength was affected to a lesser extent (factor of 1.4). Similar variations in strength when isospin is included in the statistical

calculation have been observed in the case of ${}^{63}\text{Cu}$ [11]. In the case of lighter nuclei near $A = 40$, however, the effect of isospin on the GDR width and energy is larger [10]. Rather than fit all the spectra with the isospin-dependent version, which requires considerably more computing time (factor of 4 or more) than the normal version, we have instead inferred strength corrections from the comparisons above. All quoted GDR strengths have been corrected for isospin by the factors given above.

C. Level density

One of the most critical elements in the decay scheme calculated by CASCADE is the level density. In general, an analytic function parametrizes the level density in terms of a parameter a (which determines the energy dependence) and a pairing energy Δ (which effectively redefines the zero point of excitation energy). The level-density formula for excitation energy E_x and spin J is given by:

$$\rho(U(E_x, J)) = \frac{\sqrt{a}}{12\Theta^{3/2}} \frac{2J+1}{(U+T)^2} \exp(2\sqrt{aU}), \quad (4)$$

where the effective excitation energy U accounts for the rotational and pairing energies and can be related to the nuclear temperature T by an equation of state:

$$U(E_x, J) = E_x - E_{\text{rot}}(J) - \Delta = aT^2 - T. \quad (5)$$

The spin dependence enters in the form of an yrast line $E_{\text{rot}}(J) = J(J+1)/\Theta$, where $\Theta = \Theta_0(1 + \delta J^2 + \delta' J^4)$, $\Theta_0 = 2I_0/\hbar^2$, and the spherical rigid-body moment of inertia $I_0 = \frac{2}{5}M(r_0 A^{1/3})^2$. The parameters δ and δ' account for the deformability of a rotating liquid drop [33].

In view of the tremendous range of excitation energies spanned in the calculation, four separate energy regions are defined for the level densities [18]. Below $E_x \sim 5$ MeV, individual levels are enumerated. In the ‘‘low’’ energy region ($5 \text{ MeV} \leq E_x \leq 40 A^{-1/3} \text{ MeV}$), the parameters a and Δ have been compiled from experimental work (low-energy resonance studies and near-threshold neutron capture data) for many nuclei [34,35], and where unavailable, can be estimated from a fit to the empirical data by Dilg *et al.* [34] using a ‘‘back-shifted’’ Fermi gas model [35–37]. In the ‘‘high’’ energy region ($E_x \geq 80 A^{-1/3}$), it is assumed that shell and pairing effects vanish [38,39], allowing a smooth mass dependence to be inferred for a and Δ consistent with the liquid-drop model. In this case, $a = A/8$ and Δ is determined by the ground-state energy of spherical liquid drop (derived from the Myers-Swiatecki mass formula [40]). In the transition region between these two domains, a linear interpolation is applied to the level-density parameters.

A problem arises for this parametrization if the matching between the ‘‘low’’ and ‘‘high’’ energy regimes is not smooth. A sudden slope variation in the transition region can introduce inconsistencies in the γ -ray spectrum for high-energy decays ($E_\gamma > 15$ MeV) that populate states in this region. Reisdorf [41] has developed a semiempirical level-density formula included in his statistical code HIVAP which circumvents this difficulty by utilizing an

energy-dependent parameter a (explicitly accounting for shell and pairing effects) over the entire excitation energy range. His level density is given by Eq. (4) above, by replacing $(U + T)^2$ in the denominator by U^2 and defining a by:

$$aU = \bar{a} \{ U + \delta U [1 - \exp(-\gamma U)] \}, \quad (6)$$

where $U(E_x, J) = E_x - E_{\text{rot}}(J) + \delta P$, and δU and δP are the shell and pairing corrections. Here the spin dependence of Θ is neglected. The smooth quantity \bar{a} corresponds closely to the conventional level-density parameter and has been calculated by Reisdorf [41] in a microscopic formulation. The shell corrections δU are exponentially damped out at higher energies by the factor γ , which is given by $\gamma^{-1} = 18.5$ MeV. Unlike the Pühlhofer approach, where results are sensitive to the “free” parameter a which is not well determined, the Reisdorf approach provides an unambiguous value of \bar{a} and gives results for medium-weight nuclei that are insensitive to the value of γ , as seen in recent studies of GDR’s in ^{63}Cu [11] and in $A = 39\text{--}45$ nuclei [10]. In that respect, this level density is physically more tractable over a broad range of excitation energies.

1. Pühlhofer prescription

In the present work, we have used both the Pühlhofer and Reisdorf formulations of the level density. First we consider the Pühlhofer prescription. Whereas the level density in the “low” energy region is reasonably well determined by the empirical parameters of Dilg *et al.* [34] and Vonach and Hille [35], the parameters a and Δ in the “high” energy liquid-drop region are not so pre-

cisely known. We have performed CASCADE calculations for several values of the parameter a (ranging from $A/7$ to $A/10$) and for Δ with and without the so-called Wigner term [40]. The sensitivity of the results to the level density is demonstrated in Fig. 2, where we have plotted the GDR parameters as a function of the level-density parameter for the $\alpha + ^{48}\text{Ti}$ reaction at $E_\alpha = 28$ MeV and the $^{19}\text{F} + ^{27}\text{Al}$ reaction at $E(^{19}\text{F}) = 50$ MeV.

The $\alpha + ^{48}\text{Ti}$ reaction shows a very strong sensitivity to the level density. This effect may be understood by referring to Fig. 3, where the ^{52}Cr level-density curve is depicted for different parametrizations. As discussed above, γ decays that populate states in the transition region ($E_x \sim 11\text{--}22$ MeV in this case) are affected by the sudden slope variation from the “high” energy liquid-drop regime (with $a = A/8$). However, unlike the situation in $A \sim 40$ nuclei [10], these slope variations are not so pronounced as to preclude using the Pühlhofer formulation after some parameter adjustments. As seen in Fig. 3, the curve for $a = A/8.5$ and Δ including the Wigner term offers a smoother and more physically realistic alternative to the CASCADE default of $a = A/8$.

The sensitivity to this problem is significantly reduced in the case of $^{19}\text{F} + ^{27}\text{Al}$. Decays from this compound system originate at much higher energy and therefore do not enter the transition region in the first stages of the deexcitation cascade, where the GDR plays an important role. The level-density curves for ^{46}Ti are similar to the ones in Fig. 3. The slope differences between the various curves above 22 MeV are quite subtle, and this is reflected in the smaller variation in the GDR parameters extracted using different level densities.

The systematic variation of the GDR energy and strength with the parameter a may be understood by re-

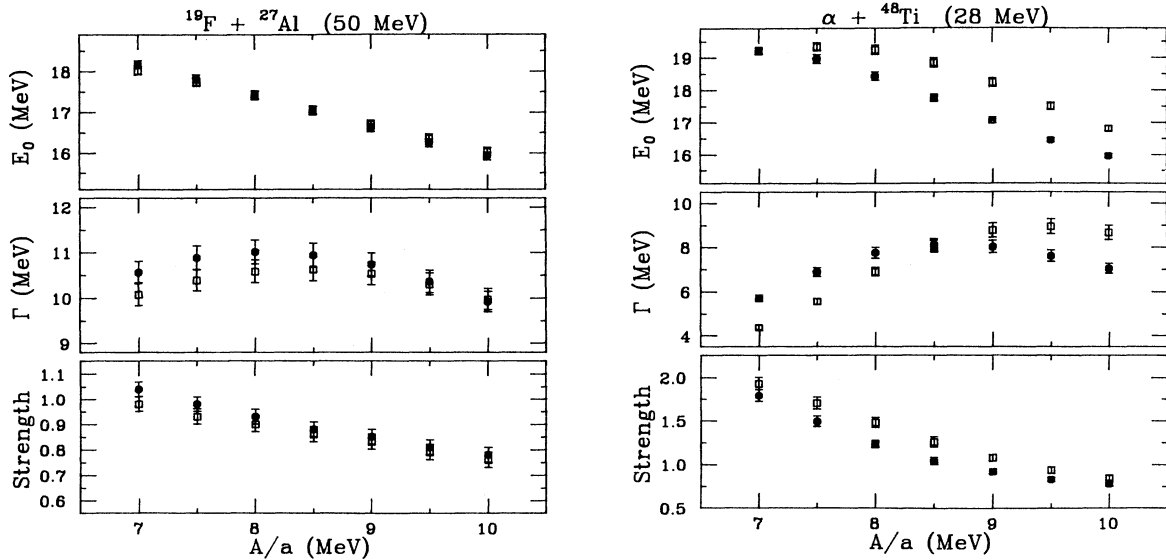


FIG. 2. Effect of the liquid-drop level-density parameters in the Pühlhofer prescription on the fitted GDR parameters for the $^{19}\text{F} + ^{27}\text{Al}$ reaction at $E(^{19}\text{F}) = 50$ MeV (left panel) and for the $\alpha + ^{48}\text{Ti}$ reaction at $E_\alpha = 28$ MeV (right panel). The solid circles represent calculations with Δ including the Wigner term, and the open squares do not include the Wigner term.

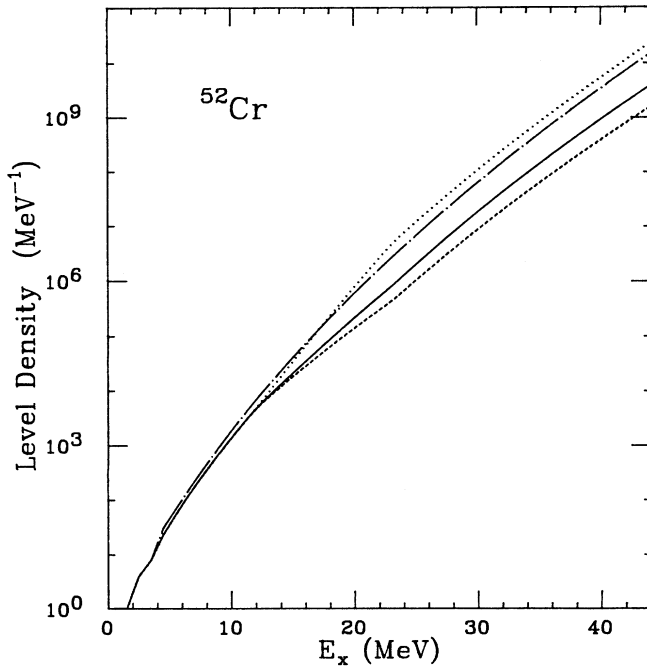


FIG. 3. Level density for ^{52}Cr determined using the Pühlhofer formula with different parameters and using the Reisdorf formula (dot-dashed curve). The Pühlhofer curves are identified as follows: $a = A/8$ (dots), $a = A/8.5$ and Δ including Wigner term (solid), and $a = A/9$ and Δ including Wigner term (dashes).

calling the level-density expression in Eq. (4). The slope of the level-density curve is largely determined by the parameter a in the exponential term. A steeper slope (corresponding to larger values of a) means that high-energy γ decay competes less favorably with low-energy particle emission, thus requiring a higher GDR energy and larger strength to fit the data, as seen in Fig. 2.

The problem of selecting the best level-density parameters for the Pühlhofer prescription is difficult. Some parameter combinations could be excluded on the basis of poor spectrum fit quality, but many could not. In order

to further constrain the level-density parameters, some restriction on the acceptable GDR parameter values was necessary. Fortunately, there are firm theoretical calculations (plus supporting results from other experiments [23]) that suggest that the GDR energy and strength should be independent of temperature and spin [42–45]. With these additional constraints, the best compromise was achieved with $a = A/8.5$ and Δ including the Wigner term. Having to employ such constraints, however, means that we cannot draw any firm conclusions from this part of the analysis about the stability of E_0 and S as a function of temperature and spin.

The statistical-model fits to the γ -ray spectra are shown by the solid lines in Fig. 1. The calculated curves provide a good description of the data over a cross section range of 6–7 orders of magnitude. The resulting GDR parameters are listed in Table II. The errors quoted in the table reflect variations in the fit results due to a range of values $a = A/8.5 \pm 0.5$ for the level-density parameter.

2. Reisdorf prescription

The difficulties described above led us to explore the level-density approach developed by Reisdorf [41]. Here the shell and pairing effects are damped out smoothly from low to high excitation energy, and the smooth parameter \bar{a} is calculated from theory. In addition, there is the damping factor γ , to which the statistical calculations are highly insensitive. This level-density prescription has been compared to variations of the Pühlhofer prescription in a recent study of statistical decays in ^{63}Cu [11]. Figure 3 shows the Reisdorf level-density curve for ^{52}Cr , which can be seen to have a much smoother variation with energy compared to the other curves. Fits to the present data using this formulation are shown in Fig. 4, and the resultant GDR parameters are summarized in Table II. It should be mentioned that our analysis using the Reisdorf level density was performed with the same level-density parameters as for ^{63}Cu [11]. This was reasonable because the ground-state shell effects for the nuclei presently studied and the ^{63}Cu nucleus are not so different, and the experimental values of the level spacing

TABLE II. GDR parameters deduced from the statistical-model analysis using the Pühlhofer level density (with $a = A/8.5$ and Δ including the Wigner term) and the Reisdorf level density. E_{xi} is the initial compound nucleus excitation energy. The determination of the mean final-state spin $\langle J_f \rangle$ and effective final-state temperature $\langle T_f \rangle$ is discussed in the text. Strengths have been corrected for isospin.

Reaction	E_{xi} (MeV)	$\langle T_f \rangle$ (MeV)	$\langle J_f \rangle$ (\hbar)	Pühlhofer level density				Reisdorf level density			
				E_0 (MeV)	Γ (MeV)	S	χ^2	E_0 (MeV)	Γ (MeV)	S	χ^2
$\alpha + ^{48}\text{Ti}$	35.2	1.36	9.3	17.9 ± 0.7	8.2 ± 0.5	1.04 ± 0.16	1.8	18.7 ± 0.1	6.5 ± 0.2	1.04 ± 0.03	3.5
	31.5	1.26	8.4	17.7 ± 0.5	8.1 ± 0.5	0.84 ± 0.10	1.5	18.1 ± 0.1	5.6 ± 0.2	0.94 ± 0.03	4.3
	25.2	0.89	6.5	17.9 ± 0.2	6.9 ± 0.4	0.70 ± 0.04	0.7	17.6 ± 0.2	5.9 ± 0.3	1.02 ± 0.05	1.3
	20.4	0.51	4.5	17.7 ± 0.5	7.0 ± 1.0	0.75 ± 0.15	...	17.7 ± 0.5	6.0 ± 1.0	1.10 ± 0.15	...
$^{19}\text{F} + ^{27}\text{Al}$	58.1	1.50	18.2	16.8 ± 0.4	12.2 ± 0.5	0.88 ± 0.06	1.4	18.0 ± 0.1	12.8 ± 0.2	1.17 ± 0.02	2.7
	52.0	1.67	13.9	17.1 ± 0.4	10.9 ± 0.3	0.88 ± 0.06	0.6	17.9 ± 0.1	11.4 ± 0.3	1.10 ± 0.03	0.9
	46.8	1.85	8.2	17.1 ± 0.3	9.5 ± 0.3	0.86 ± 0.04	1.5	17.7 ± 0.1	10.0 ± 0.3	1.01 ± 0.03	1.9
	42.5	1.93	3.4	16.9 ± 0.8	12.0 ± 2.0	1.09 ± 0.15	0.6	18.0 ± 0.6	12.6 ± 2.0	1.21 ± 0.14	0.6

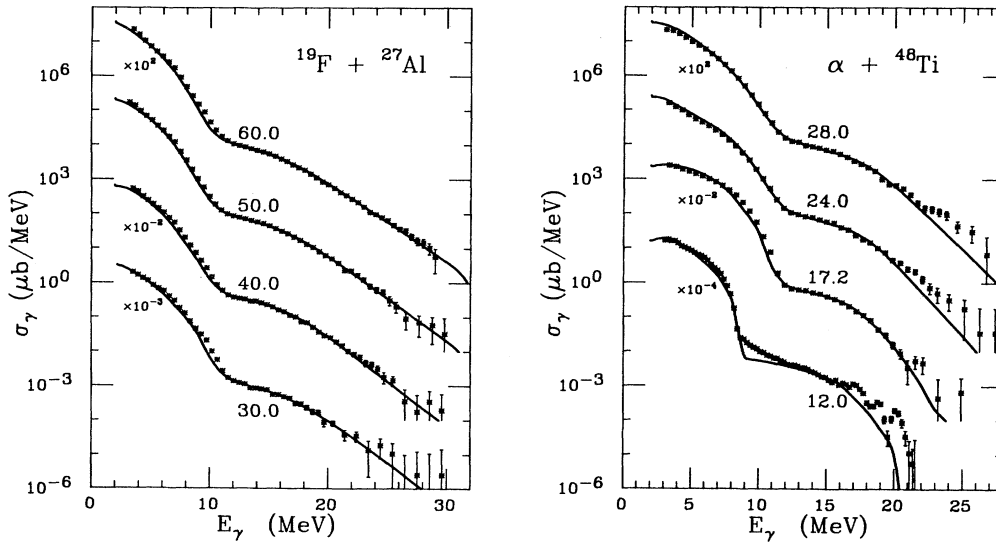


FIG. 4. Measured inclusive γ -ray spectra at $\theta_\gamma = 90^\circ$ for the $^{19}\text{F} + ^{27}\text{Al}$ reaction at $E(^{19}\text{F}) = 60, 50, 40,$ and 30 MeV (left panel) and for the $\alpha + ^{48}\text{Ti}$ reaction at $E_\alpha = 28, 24, 17.2,$ and 12 MeV (right panel). These are the same data as in Fig. 1. The solid curves are CASCADE statistical-model fits using the Reisdorf level-density formulation.

for these nuclei are sufficiently reproduced in the Reisdorf prescription with these parameters (see Figs. 3 and 4 in Ref. [10]).

The analysis with the Reisdorf level-density formulation has a significant impact on the results for the $\alpha + ^{48}\text{Ti}$ cases. Visual inspection of the calculated curves reveals a diminished fit quality for $E_\alpha = 28$ and 24 MeV, as confirmed by the higher χ^2 values. The GDR energies show a variation with excitation energy, and the widths are $\sim 1\text{--}2$ MeV smaller than those obtained using the Pühlhofer formula. These differences are mostly related to the effective Reisdorf level-density parameter $\bar{a} = A/7.9$ for ^{52}Cr . The sign of these differences can be inferred from Fig. 2, in which the width drops and the strength increases for higher a values.

One cannot infer from these fits that the Reisdorf level-density prescription is inferior to the “tuned” Pühlhofer prescription for these nuclei. The reason is that α -induced high-energy γ -ray production may have a non-negligible nonstatistical component at high E_γ for the $E_\alpha = 24$ and 28 MeV cases, as has been found for α -induced reactions on heavier nuclei at similar energies [23,46]. The $E_\alpha = 24$ MeV angular distribution (see below) offers some suggestion that nonstatistical contributions may be important here also.

The analysis of $^{19}\text{F} + ^{27}\text{Al}$ is less affected by the different level density. The GDR energies are ~ 1 MeV higher, the widths are ~ 0.5 MeV larger and the strengths are $\sim 20\text{--}30\%$ larger with the Reisdorf formula, in which $\bar{a} = A/7.7$ for ^{46}Ti . Nevertheless, the fit quality is still acceptable for all spectra, and the trend of the GDR parameters with excitation energy is preserved. Similar success in fitting statistical decay spectra for high-energy γ rays emitted in reactions in this mass region has been reported in Refs. [10,11] using the Reisdorf level density.

D. Angular distribution measurements

An angular asymmetry about $\theta_\gamma = 90^\circ$ in the center-of-mass γ -radiation distribution is a model-independent indication of a nonstatistical reaction process [23]. A purely statistical decay involves averaging over many initial states of the thermally equilibrated compound system, hence interferences between radiations of opposite parity, which can give rise to an asymmetry, should cancel out. The existence of an asymmetry would require a phase coherence between the decaying states of differing parity, and therefore the decaying system would not be in statistical equilibrium.

In order to test the assumption of statistical decay in the fusion reactions, data were obtained at five lab angles (from 40° to 140°) for selected energies in these reactions. Three such cases were examined: the $^{19}\text{F} + ^{27}\text{Al}$ reaction at $E(^{19}\text{F}) = 60$ MeV and the $\alpha + ^{48}\text{Ti}$ reaction at $E_\alpha = 17.2$ and 24 MeV. Over the course of each measurement, conditions were maintained as stable as possible (for example, data collection rate) so as to assure that no false asymmetry would arise due to external factors.

The data were treated in the same manner as previously described, with the additional procedure of accounting for Doppler shifts in γ -ray energy and converting the laboratory cross section and angle into the center-of-mass (c.m.) system. The most significant corrections occurred in the 60 MeV $^{19}\text{F} + ^{27}\text{Al}$ case, where maximum E_γ shifts of $\pm 2.6\%$ and maximum cross section conversion factors of $\pm 5\%$ were applied at the extreme angles (40° and 140°), and angular shifts were between 1.2° and 1.9° . Although these corrections appear small, they have an important effect on the extracted angular distribution coefficients.

The spectra were subsequently divided into E_γ bins of 1 MeV width. The bin yields were plotted as a function

of c.m. angle and then fitted by a sum of Legendre polynomials $P_l(\cos\theta)$:

$$W(\theta) = A_0[1 + a_1 P_1(\cos\theta) + a_2 P_2(\cos\theta)] . \quad (7)$$

The results of the angular distribution fits are shown in Fig. 5 for the three cases studied. For the ^{19}F case and the $E_\alpha = 17.2$ MeV case, the very small value of the a_1 coefficient, which is a measure of the angular asymmetry about $\theta_\gamma = 90^\circ$, is consistent with zero and hence with the assumption of a statistical decay mechanism. For the $E_\alpha = 24$ MeV case, on the other hand, the a_1 coefficient appears to be nonzero above $E_\gamma \sim 15$ MeV, which implies some nonstatistical contribution.

In the $^{19}\text{F} + ^{27}\text{Al}$ reaction at $E(^{19}\text{F}) = 60$ MeV, it is worth noting that the a_2 coefficient is slightly negative below the GDR energy and becomes positive above the GDR energy. This type of behavior for a_2 is expected for a rotating nucleus with a preferred deformation [1] and indicates that the short axis of the deformed nucleus is aligned along the spin direction, suggesting either oblate

noncollective or prolate collective rotation (for an axially symmetric system). A similar energy dependence for the a_2 coefficient was observed in the $^{18}\text{O} + ^{27}\text{Al}$ reaction at comparable spin [10]. Recent results on decays of ^{90}Zr and ^{92}Mo have been compared to thermal averaging calculations and have demonstrated that this type of anisotropy is the result of oblate noncollective deformation which increases with spin [4].

IV. INTERPRETATION OF GDR PARAMETERS

The GDR parameters from Table II for the Pühlhofer level density and the Reisdorf level density have been plotted in Fig. 6 as a function of mean final-state spin $\langle J_f \rangle$. The relevant quantities to characterize the final state populated by GDR γ decay are described below. The mean final-state energy $\langle E_{x_f} \rangle$ was computed by averaging over all steps in the decay cascade. The average final-state energy populated by GDR γ decay in the j th daughter is given by:

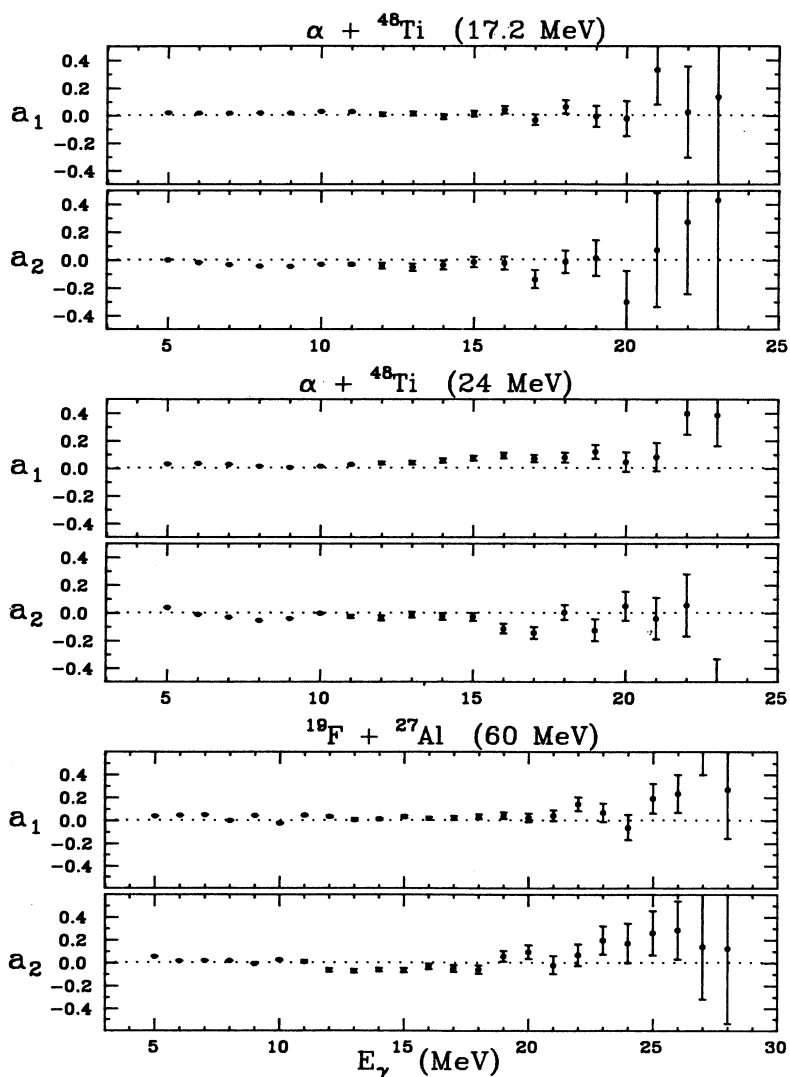


FIG. 5. Angular distribution coefficients for the $\alpha + ^{48}\text{Ti}$ reaction at $E_\alpha = 17.2$ and 24 MeV and for the $^{19}\text{F} + ^{27}\text{Al}$ reaction at $E(^{19}\text{F}) = 60$ MeV. The Legendre coefficients a_1 and a_2 are plotted as a function of γ -ray energy, where $W(\theta) = A_0[1 + a_1 P_1(\cos\theta) + a_2 P_2(\cos\theta)]$.

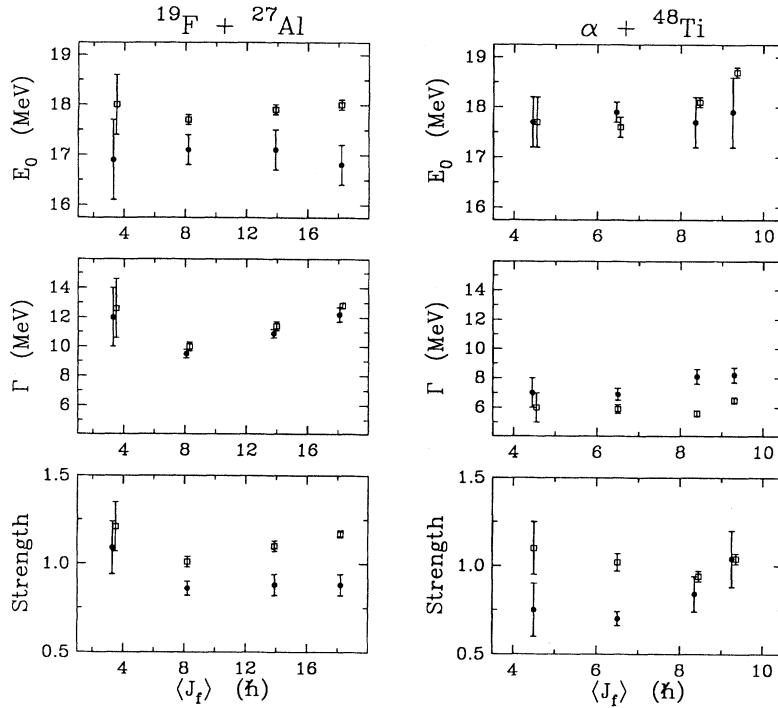


FIG. 6. Summary of fitted GDR parameters from statistical-model analyses using the Pühlhofer level density (solid circles) and the Reisdorf level density (open squares), plotted as a function of the average spin $\langle J_f \rangle$ of final states populated by γ decay. Strengths have been corrected for isospin.

$$\begin{aligned} \langle E_{x_f}(j) \rangle &= \langle E_{x_i}(j-1) \rangle - \langle E_K(j-1) \rangle \\ &\quad - E_B(j-1) - E_0, \end{aligned} \quad (8)$$

where E_B and $\langle E_K \rangle$ refer to the binding and average kinetic energies of the emitted particle (n, p, α) which populates the j th daughter, and E_0 is the GDR energy. The average of $E_{x_f}(j)$ weighted by the partial γ -ray cross section at $E_\gamma \sim E_0$ in the j th daughter yielded $\langle E_{x_f} \rangle$.

The mean final-state spin $\langle J_f \rangle$ was also computed by averaging over the daughter nuclei that contributed to high-energy γ decay. The values obtained in this way are only slightly less (by $\leq 1\hbar$) than the mean initial spin. The fact that the nuclear spin changes so little is a consequence of the enhanced probability of high-energy γ emission (relative to particle emission) in the early decay steps; evaporation of protons or α particles tends to carry off larger amounts of angular momentum. The rotational energy was computed from $\langle J_f \rangle$ by means of the following:

$$E_{\text{rot}}(J) = \frac{J(J+1)}{\Theta} = \frac{36J(J+1)}{A^{5/3}} \frac{\Theta_0}{\Theta} \text{ MeV}, \quad (9)$$

where Θ_0 is the spherical rigid-body moment of inertia and Θ is the rotating liquid-drop moment of inertia obtained from Ref. [33]. Finally, the effective nuclear temperature of the states populated by γ decay was estimated in terms of the excitation energy above the yrast line by approximating Eq. (5) as $\langle E_{x_f} \rangle - E_{\text{rot}} \approx aT^2$ with $a = A/8.5$.

Referring now to Table II and Fig. 6 for the results using the Reisdorf level density, we see that for each reaction, the resonance energies are roughly constant with ex-

citation energy and spin, in agreement with theoretical predictions [42–45]. The exception of $E_\alpha = 28$ MeV (and perhaps 24 MeV) may be distorted by nonstatistical contributions as discussed above. The sum rule strengths are also observed to be independent of excitation energy and spin, and in almost all cases are within 20% of a full $E1$ sum rule. For the analysis with the Pühlhofer level density, the approximate constancy of the resonance energy and strength (for a given reaction) is partly a consequence of our level-density parameter selection. For these results, the physically interesting quantities are the width and the magnitudes of the average resonance energies and strengths. The differences between these values and the ones obtained using the Reisdorf level density are indicative of systematic analysis uncertainties.

The width of the GDR is expected to increase with temperature [47] due to thermal averaging over an ensemble of deformations in the decaying nuclei. For the α -induced reactions, the width increase is very slight, but the variation of temperature and spin in the present range of energies is also not very extensive.

Because the ^{19}F reactions are nearly mass symmetric, the entrance channel brings in so much spin relative to the center-of-mass kinetic energy that the temperature does not increase for higher final-state energies (higher bombarding energies). On the basis of temperature considerations alone, the GDR width here should not change since the temperature does not vary significantly. Thus, the observed broadening from $E(^{19}\text{F}) = 40$ to 60 MeV can be attributed to the increase in spin. The higher spin is expected to produce an increasingly deformed oblate shape for the rotating compound nucleus [33]. If the splitting of the GDR due to this deformation is not

resolved in the spectrum shape, as is the case here, then the deformation will give rise to a strength function with a larger apparent width. Based on Fig. 10 of Ref. [33], a spin of $\langle J_f \rangle = 18.2\hbar$ implies a deformation of $\Delta R/R \sim 0.156$, and since $\Delta R/R \sim \Delta E/E_0$ we therefore infer a broadening of $\Delta E = 2.65 - 2.8$ MeV for the present range of spins in $^{19}\text{F} + ^{27}\text{Al}$, which is comparable to the width increase shown in Fig. 6. A similar effect was observed in the $^{18}\text{O} + ^{27}\text{Al}$ reaction [10].

There is a slight overlap in the spin range of the two reactions studied, namely, near $\langle J_f \rangle = 8\hbar$ and below. At these spins, the widths obtained in the ^{19}F reactions are larger than the widths from the α -induced reactions, presumably attributable to the higher final-state temperatures which give rise to larger thermal shape fluctuations.

The present results can be compared to other measurements in neighboring nuclei at similar temperature and spin. In the $^{18}\text{O} + ^{27}\text{Al}$ reaction [10], widths varied from 11.6 to 14.7 MeV for $\langle J_f \rangle \sim (8 - 18.5)\hbar$ and $\langle T_f \rangle \sim 1.7$ MeV. While the trend of increasing width with increasing spin is consistent with the present results for $^{19}\text{F} + ^{27}\text{Al}$, the widths are ~ 2 MeV larger in the $^{18}\text{O} + ^{27}\text{Al}$ case. This comparison leads to an interesting observation. In the $^{19}\text{F} + ^{27}\text{Al}$ analysis, if we were to ascribe the problem in reproducing the low-energy yield to a normalization error rather than an error in the fusion cross section (see Sec. III A), then using measured fusion cross sections [18,28], the deduced average final-state spins for the three highest bombarding energy cases would be lower ($\langle J_f \rangle = 14.6\hbar, 12.1\hbar, 7.4\hbar$ instead of $\langle J_f \rangle = 18.2\hbar, 13.9\hbar, 8.2\hbar$ —see Table II) and the widths observed here would fit well with the (spin-dependent) widths obtained for $^{18}\text{O} + ^{27}\text{Al}$ [10]. With these lower spins, the deduced average final-state temperatures would not drop with bombarding energy (see Table II) but would be approximately constant at $\langle T_f \rangle \sim 1.8$ MeV, similar to Ref. [10]. From the present work, we do not know which scenario is correct, and we regard the spread in spin and temperature values determined by these two methods to be representative of our uncertainty in these quantities.

The small width increase observed in the α -induced reactions is in agreement with results obtained for the $\alpha + ^{59}\text{Co}$ reaction at $\langle J_f \rangle \sim (5 - 8)\hbar$ and $\langle T_f \rangle \sim 0.7 - 1.2$ MeV [11]. In that case, the widths were in the range 7.5–8 MeV with very little variation over the spin and temperature range studied, as observed in the present work. Ground-state GDR widths measured in (γ, n) reactions on ^{46}Ti [48], ^{50}Ti [49], and ^{52}Cr [50] are all $\Gamma \sim 5 - 6$ MeV. Thus all our observed GDR widths for both the $\alpha + ^{48}\text{Ti}$ and the $^{19}\text{F} + ^{27}\text{Al}$ reactions are broader than the ground-state GDR widths.

Entrance channels involving stable targets and projectiles of mass $A \geq 4$ will only populate the lower isospin component of the GDR. The location of the $T_<$ component of the GDR in ^{46}Ti and ^{52}Cr can be estimated

based on systematics of the GDR energy and the shift predicted by the isospin splitting model [51,52]. For ^{46}Ti , this gives a GDR centroid of 19.6 MeV and a $T_<$ component at 18.4 MeV. For ^{52}Cr , the centroid is at 19.0 MeV, with the $T_<$ component at 18.1 MeV. In the present analysis, the energies obtained using the Reisdorf level density are lower than these estimates by ~ 0.5 MeV or less on average. Using the Pühlhofer level density, the level of agreement for ^{52}Cr is similar, but the results for the ^{46}Ti case are considerably worse, differing by more than 1 MeV in all instances.

V. SUMMARY AND CONCLUSIONS

We have studied the GDR built on excited states in ^{46}Ti and ^{52}Cr through fusion-evaporation reactions. In the reactions $^{19}\text{F} + ^{27}\text{Al} \rightarrow ^{46}\text{Ti}$ and $\alpha + ^{48}\text{Ti} \rightarrow ^{52}\text{Cr}$, the statistical model reproduced the measured inclusive γ -ray spectra quite well from $E_\gamma \sim 5$ to 30 MeV, spanning more than six orders of magnitude in yield. The role of isospin in these light compound systems was seen to be important for determining the GDR strength. The apparently low values of the resonance energy deduced in this analysis could also be understood in terms of isospin, since the entrance channel only populates the $T_<$ GDR component. The large observed widths arise presumably from thermal averaging over an ensemble of deformations at moderate excitation energy and spin.

The nearly mass-symmetric case of $^{19}\text{F} + ^{27}\text{Al}$ differs from the usual situation in which the temperature increases with bombarding energy—here the temperature decreased with increasing bombarding energy, and thus the observed broadening of the resonance was identified as being due to the increase in spin, consistent with expectations based on the rotating liquid-drop model.

Two level-density parametrizations were investigated in the present work. From the results, it is clear that the limitations of the Pühlhofer formulation make it necessary to adjust certain critical parameters without an independent check on the adjustable factors, thus rendering it rather unsatisfactory. The analysis with the Reisdorf level density was performed with parameters used for heavy and medium-weight nuclei [11] and resulted in reasonable fits, with somewhat higher χ^2 values, however. Further improvement in this analysis might be possible based on improved Reisdorf level-density parameters as determined in Ref. [10].

Having obtained a reasonable understanding and description of the statistical decay process in these nuclei, the present results and analysis form an adequate basis for calculating the statistical contribution to the (p, γ) reactions populating the same residual nuclei. The results of these (p, γ) studies will be the subject of a forthcoming paper [13].

- [1] K. A. Snover, Nucl. Phys. **A482**, 13c (1988).
- [2] J. J. Gaardhøje, A. M. Bruce, and B. Herskind, Nucl. Phys. **A482**, 121c (1988).
- [3] J. J. Gaardhøje and A. Maj, Nucl. Phys. **A520**, 575c (1990).
- [4] J. H. Gundlach, K. A. Snover, J. A. Behr, C. A. Gossett, M. Kicińska-Habior, and K. T. Lesko, Phys. Rev. Lett. **65**, 2523 (1990).
- [5] R. Butsch, M. Thoennessen, D. R. Chakrabarty, M. G. Herman, and P. Paul, Phys. Rev. C **41**, 1530 (1990).
- [6] M. Thoennessen, D. R. Chakrabarty, R. Butsch, M. G. Herman, P. Paul, and S. Sen, Phys. Rev. C **37**, 1762 (1988).
- [7] D. R. Chakrabarty, M. Thoennessen, S. Sen, P. Paul, R. Butsch, and M. G. Herman, Phys. Rev. C **37**, 1437 (1988).
- [8] M. Kicińska-Habior, K. A. Snover, J. A. Behr, C. A. Gossett, J. H. Gundlach, and G. Feldman, Phys. Rev. C **45**, 569 (1992).
- [9] C. A. Gossett, K. A. Snover, J. A. Behr, G. Feldman, and J. L. Osborne, Phys. Rev. Lett. **54**, 1486 (1985).
- [10] M. Kicińska-Habior, K. A. Snover, J. A. Behr, G. Feldman, C. A. Gossett, and J. H. Gundlach, Phys. Rev. C **41**, 2075 (1990).
- [11] M. Kicińska-Habior, K. A. Snover, C. A. Gossett, J. A. Behr, G. Feldman, H. K. Glatzel, J. H. Gundlach, and E. F. Garman, Phys. Rev. C **36**, 612 (1987).
- [12] M. N. Harakeh, D. H. Dowell, G. Feldman, E. F. Garman, R. Loveman, J. L. Osborne, and K. A. Snover, Phys. Lett. **176B**, 297 (1986).
- [13] G. Feldman, J. A. Behr, C. A. Gossett, J. H. Gundlach, M. Kicińska-Habior, K. A. Snover, D. H. Dowell, and A. M. Sandorfi (unpublished).
- [14] M. Hasinoff, S. T. Lim, D. F. Measday, and T. J. Mulligan, Nucl. Instrum. Methods **117**, 375 (1974).
- [15] D. H. Dowell, C. A. Gossett, and K. A. Snover, University of Washington Nuclear Physics Laboratory Annual Report, 1984 (unpublished), p. 78.
- [16] H. K. Glatzel, Diplomarbeit, University of Mainz, 1986 (unpublished).
- [17] W. R. Nelson, H. Hirayama, and D. W. O. Rogers, SLAC Report No. 265, 1985 (unpublished).
- [18] F. Pühlhofer, Nucl. Phys. **A280**, 267 (1977).
- [19] W. Hauser and H. Feshbach, Phys. Rev. **87**, 366 (1952).
- [20] T. D. Thomas, Ann. Rev. Nucl. Sci. **18**, 343 (1968).
- [21] P. E. Hodgson, *Nuclear Heavy-Ion Reactions* (Oxford University Press, Oxford, 1978).
- [22] R. G. Stokstad, in *Treatise of Heavy-Ion Science*, Vol. 3, edited by D. A. Bromley (Plenum, New York, 1985).
- [23] K. A. Snover, Ann. Rev. Nucl. Part. Sci. **36**, 545 (1986).
- [24] D. M. Brink, D. Phil. thesis, Oxford University, 1955 (unpublished).
- [25] J. R. Huizenga and G. Igo, Nucl. Phys. **29**, 462 (1962).
- [26] L. C. Vaz and J. M. Alexander, in *Fusion Reactions Below the Coulomb Barrier*, edited by S. G. Steadman, Lecture Notes in Physics Vol. 219 (Springer, Berlin, 1985), p. 288; Z. Phys. A **318**, 231 (1984).
- [27] W. W. Wilcke, J. R. Birkelund, H. J. Wollersheim, A. D. Hoover, J. R. Huizenga, W. U. Schröder, and L. E. Tubbs, At. Data Nucl. Data Tables **25**, 389 (1980).
- [28] M. S. Chiou, M. W. Wu, N. Easwar, and J. V. Maher, Phys. Rev. C **24**, 2507 (1981).
- [29] C. Y. Wong, Phys. Rev. Lett. **31**, 766 (1973).
- [30] D. L. Hill and J. A. Wheeler, Phys. Rev. **89**, 1102 (1953).
- [31] Y. Eisen, I. Tserruya, Y. Eyal, Z. Fraenkel, and M. Hillman, Nucl. Phys. **A291**, 459 (1977).
- [32] N. V. Sen, R. Darves-Blanc, J. C. Gondrand, and F. Merchez, Phys. Rev. C **27**, 194 (1983).
- [33] S. Cohen, F. Plasil, and W. J. Swiatecki, Ann. Phys. (N.Y.) **82**, 557 (1974).
- [34] W. Dilg, W. Schantl, H. Vonach, and M. Uhl, Nucl. Phys. **A217**, 269 (1973).
- [35] H. Vonach and M. Hille, Nucl. Phys. **A127**, 289 (1969).
- [36] E. Gadioli and L. Zetta, Phys. Rev. **167**, 1016 (1968).
- [37] J. R. Huizenga, H. K. Vonach, A. A. Katsanos, A. J. Gorski, and C. J. Stephan, Phys. Rev. **182**, 1149 (1969).
- [38] V. S. Ramamurthy, S. S. Kapoor, and S. K. Kataria, Phys. Rev. Lett. **25**, 386 (1970).
- [39] F. C. Williams, G. Chan, and J. R. Huizenga, Nucl. Phys. **A187**, 225 (1972).
- [40] W. D. Myers and W. J. Swiatecki, Nucl. Phys. **81**, 1 (1966).
- [41] W. Reisdorf, Z. Phys. A **300**, 227 (1981).
- [42] H. Sagawa and G. F. Bertsch, Phys. Lett. **146B**, 138 (1984).
- [43] H. M. Sommermann, Ann. Phys. (N.Y.) **151**, 163 (1983).
- [44] P. Ring, L. M. Robledo, J. L. Egido, and M. Faber, Nucl. Phys. **A419**, 261 (1984).
- [45] S. Yang and Z. Szymanski, Nucl. Phys. **A436**, 397 (1985).
- [46] J. A. Behr, K. A. Snover, C. A. Gossett, G. Feldman, and J. H. Gundlach, Bull. Am. Phys. Soc. **30**, 1256 (1985); (unpublished).
- [47] M. Gallardo, M. Diebel, T. Døssing, and R. A. Broglia, Nucl. Phys. **A443**, 415 (1985).
- [48] R. E. Pywell and M. N. Thompson, Nucl. Phys. **A318**, 461 (1979).
- [49] R. E. Pywell, M. N. Thompson, and R. S. Hicks, Nucl. Phys. **A325**, 116 (1979).
- [50] J. Weise, M. N. Thompson, K. Shoda, and T. Tsubota, Aust. J. Phys. **30**, 401 (1977).
- [51] S. Fallieros and B. Goulard, Nucl. Phys. **A147**, 593 (1970).
- [52] R. O. Akyüz and S. Fallieros, Phys. Rev. Lett. **27** 1016 (1971).